

# Inhibition of electromagnetically induced absorption due to excited state decoherence in Rb vapor.

H. Failache, P. Valente, G. Ban\*, V. Lorent<sup>†</sup> and A. Lezama<sup>‡</sup>  
*Instituto de Física, Facultad de Ingeniería. Casilla de correo 30.  
11000, Montevideo, Uruguay.*  
(November 1, 2018)

The explanation presented in [Taichenachev et al, Phys. Rev. A **61**, 011802 (2000)] according to which the electromagnetically induced absorption (EIA) resonances observed in degenerate two level systems are due to coherence transfer from the excited to the ground state is experimentally tested in a Hanle type experiment observing the parametric resonance on the  $D1$  line of  $^{87}\text{Rb}$ . While EIA occurs in the  $F = 1 \rightarrow F' = 2$  transition in a cell containing only  $Rb$  vapor, collisions with a buffer gas (30 torr of  $Ne$ ) cause the sign reversal of this resonance as a consequence of collisional decoherence of the excited state. A theoretical model in good qualitative agreement with the experimental results is presented.

## I. INTRODUCTION.

There has been considerable interest in recent years for the fascinating properties of coherently prepared atomic media [1]. Among the most studied coherent effects is the phenomenon of electromagnetically induced transparency (EIT) [2]. EIT has generally been modelled and experimentally studied in three-level  $\Lambda$  systems with two long lived lower (ground) states and a rapidly decaying upper (excited) state. The two electromagnetic fields (pump and probe) separately couple each of the two arms of the  $\Lambda$  system. A distinctive feature of the EIT resonance is its narrow linewidth which corresponds to the coherence decay rate of the ground state doublet. The occurrence of the EIT resonance is directly linked to the existence of a dark state (DS): i.e. a linear combination of the two ground states uncoupled to the excited state. EIT is a consequence of the system being pumped into the DS.

EIT may also be observed in multi-level systems as those involving the Zeeman substates of two atomic levels with angular momentum degeneracy, hereafter called

degenerate two-level systems (DTLS). In such case too, the observation of EIT is a direct consequence of the existence of a DS within the lower atomic level when  $F_g \geq F_e$  ( $F_g$  and  $F_e$  are the angular momenta of the ground and excited state respectively).

The pump-probe spectroscopy of DTLS with  $0 < F_g < F_e$  also presents resonances in the probe transmission when the Raman resonance condition between ground state Zeeman sublevels is fulfilled. However, in this case, the resonances correspond to an increase of the probe absorption and have consequently being designated as electromagnetically induced absorption (EIA) [3–5]. As in the case of EIT resonances, the EIA linewidth is given by the coherence decay rate of the ground level. Unlike EIT, the EIA resonances cannot be associated to the existence of a DS in the ground state. Also, there is no simple connection between the EIA resonances and the existence of a DS in the *excited* state since such state has a lifetime limited by spontaneous emission and cannot account for the narrow spectral features observed.

An explanation for the EIA resonance was provided by Taichenachev et al [6] analyzing a four level system in a  $N$  configuration. They showed theoretically that in this system, which is the simplest to present EIA, the enhanced absorption is due to the transfer, via spontaneous emission, of the coherence created by the exciting fields within the two upper levels. Although the  $N$  configuration does not correspond to the configurations actually explored in realistic DTLS, the argument presented in [6] can be extended to such systems [7].

The purpose of this paper is to provide experimental evidence in support of the argument presented in [6] by demonstrating that EIA resonances are suppressed (and even reversed) if the coherence of the excited state is significantly destroyed by collisions before the occurrence of the spontaneous emission decay. A simple theoretical model in good agreement with the observations is also presented.

A convenient experimental scheme for the observation of coherence resonances is the Hanle type setup that uses a unique optical beam with linear polarization in near resonance with an atomic transition. In this scheme, the two opposite circular polarization components of the light can be considered as the pump and probe fields. The light beam is sent through an atomic sample where the Raman resonance condition is tuned, via the Zeeman effect, by a magnetic field along the light propagation

---

\*Permanent address: Laboratoire de Physique Corpusculaire, 14050 Caen, France.

<sup>†</sup>Permanent address: Laboratoire de Physique des Lasers, 93430 Villetaneuse, France.

<sup>‡</sup>E-mail: alezama@fing.edu.uy

axis. The intensity of the transmitted light is monitored. Hanle/EIT/EIA resonances on the  $D1$  lines of alkaline vapors were recently studied by several groups [8–13] (see inset in Fig. 4 for an energy level scheme of the  $^{87}\text{Rb}$   $D1$  line). Dancheva et al [11] were the first to observe a Hanle/EIA resonance on a  $F_g \rightarrow F_e = F_g + 1$  transition of the  $D1$  line. They pointed out the fact that the EIA resonance can be observed in spite of the transition being open (radiative decay can occur from the excited state to either ground state hyperfine levels). The open character of the transition is responsible for the smallness of the Hanle/EIA resonance as compared with the Hanle/EIT resonances occurring when  $F_e = F_g, F_g - 1$ .

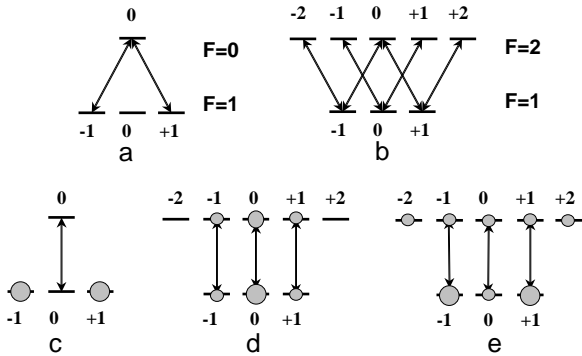


FIG. 1. Examples of energy level configurations in DTLs with a linear optical field polarization. *a* and *b*: quantization axis perpendicular to the optical polarization. *c* – *d*: quantization axis parallel to the optical polarization. The circles represent the sublevel population. *d*: no collisional relaxation of the excited state. *e*: collisionally thermalized excited state.

The choice of the Hanle experimental scheme for coherent spectroscopy is not only motivated by its simplicity. It also allows a special insight on the connection between coherence resonance and optical pumping. Consider the situation depicted in Fig. 1. Figs. 1a) and 1b) correspond to a  $F_g = 1 \rightarrow F_e = 0$  and  $F_g = 1 \rightarrow F_e = 2$  transitions respectively. In both cases, the quantization axis has been chosen parallel to the direction of the light propagation which coincides with the orientation of the magnetic field. The Raman resonance condition is achieved for the two components of the optical field at zero magnetic field and destroyed for nonzero magnetic field. In Fig.1a) the optical field interact with a  $\Lambda$  system for which EIT is known to occur as a consequence of the existence of a DS formed by the anti-symmetric combination of the ground state Zeeman sublevels  $|-1\rangle$  and  $|+1\rangle$ . The situation in Fig. 1b) corresponds to EIA which results, according to [6], from the transfer of coherence from the upper to the lower level via spontaneous emission. Figs. 1c) and 1d) represent the same physical situation than in

a) and b) respectively with the quantization axis taken along the direction of the linear polarization of the light. In Fig. 1c) the transparency observed for zero magnetic field is the consequence of the optical pumping of the system into the  $|-1\rangle$  and  $|+1\rangle$  sublevels which are not coupled to the excited state. In Fig. 1d) the absorption increase for  $B = 0$  is a consequence of the redistribution of the population of the ground state Zeeman sublevels (alignment) via optical pumping. The atomic population accumulates preferentially in the  $|0\rangle$  sublevel which has the largest coupling with the excited state. Notice that with this choice of the quantization axis, no coherence is built among the excited state Zeeman sublevels and thus cannot be transferred to the ground state. In the basis used in c) and d) the Hanle/EIT and Hanle/EIA resonances appear as a consequence of incoherent optical pumping.

Since the choice of the quantization axis is arbitrary, the two frames considered in the previous discussion can conveniently be considered for the analysis of the Hanle/EIA resonances under the effect of collisions affecting the excited state. In the scheme of Fig. 1b) which can be considered as an extension of the simple  $N$  system analyzed by Taichenachev et al [6], EIA is a consequence of the spontaneous transfer of Zeeman coherence from the excited to the ground state. In consequence, the EIA resonance should disappear if the excited state coherence is destroyed by collisions in a time comparable or shorter than the excited state lifetime. In the basis corresponding to Fig. 1d) EIA can be prevented if the collisions are responsible for a significant equalization (thermalization) of the excited state sublevel populations before the occurrence of spontaneous emission (Fig. 1e). If the excited state is completely thermalized then the total spontaneous emission decay into a given ground state Zeeman sublevel is the same for all ground state sublevels. In consequence, in the steady state, the population is preferentially accumulated in sublevels  $|\pm 1\rangle$  resulting in an increased transparency.

To demonstrate the influence of the excited state coherence on EIA we have observed the Hanle/EIT/EIA resonances corresponding to the four transitions of the  $D1$  line of  $^{87}\text{Rb}$  both in a vapor cell containing only Rb vapor (negligible collisions) and in a cell containing 30 torr of Ne as buffer gas.

It is well known that room temperature collisions with light noble gas atoms (He, Ne, Ar) produce different effects on the  $^2S_{1/2}$  ground state than in the  $^2P_{1/2}$  or  $^2P_{3/2}$  excited states of several alkaline vapors [14]. The collisions of a noble gas atom with an alkaline atoms in its ground state has little effect on its electronic and nuclear spin. As a consequence the alkaline atom can experience a very large number of collisions while preserving the ground state coherence. However, the atomic motion is affected by collisions becoming diffusive. This results in a longer interaction time before the atoms can leave the

light beam or reach the cell walls. The increased interaction time allows the observation of coherence resonances with time-of-flight limited linewidth of only a few tenths of  $Hz$  [15–17].

The situation is rather different for collisions between noble gas atoms and alkaline atoms in the  $^2P_{1/2}$  state [14]. At room temperature and for the buffer gas density corresponding to the experiments described below, the collisions are sufficiently energetic and frequent to produce a considerable broadening of the homogeneous width of the optical transitions (which remains nevertheless smaller than the Doppler width and the  $^2P_{1/2}$  hyperfine splitting). Also under such conditions virtual transitions to the neighboring levels (mainly  $^2P_{3/2}$ ) occur [18,19] resulting in the non preservation of the magnetic quantum number ( $m_J$ ) of the electronic angular momentum during collisions. As a consequence, a significant thermalization of the excited state density matrix take place in a time shorter than the excited state lifetime. The cross section for excited state collisional  $m_J$  mixing was measured by several authors [18–21]. Using the figures in [19] and the Ne density corresponding to the experiments the collisional decoherence rate of the excited state  $\gamma_{coll}$  can be estimated as  $\gamma_{coll} \approx 4\Gamma$  where  $\Gamma$  is the excited state spontaneous emission decay rate.

## II. EXPERIMENT

The experimental setup is shown in Fig. 2. We have used two cylindrical vapor cells of the same dimensions (diameter:  $2.5\text{ cm}$ , length:  $5\text{ cm}$ ) provided by the same manufacturer and filled with natural rubidium vapor. One of the cells contains  $30\text{ torr}$  of Ne as buffer gas. The cell under consideration was placed (at room temperature) inside a magnetic shield formed by three coaxial cylindrical  $\mu$ -metal layers. After degaussing of the  $\mu$ -metal shield the total inhomogeneity of the residual magnetic field at the vapor cell was less than  $10\ \mu G$ . A coaxial solenoid, internal to the magnetic shield was used to scan the magnetic field at the atomic sample.

An extended cavity diode laser ( $\sim 1\text{ MHz}$  linewidth) was used for the atomic excitation. The laser frequency was monitored and stabilized on specific hyperfine transitions with the help of an auxiliary saturated absorption setup. The total laser power at the sample was approximately  $0.1\text{ mW}$ . The light transmitted through the vapor cell was monitored with a photodiode ( $100\text{ kHz}$  bandwidth).

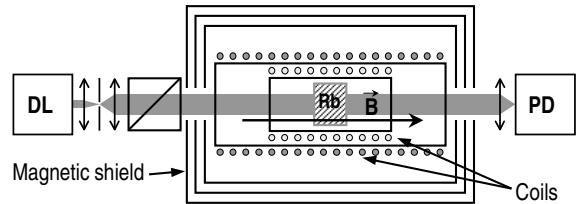


FIG. 2. Experimental setup. DL: diode laser. PD: photodiode.

In order to enhance sensitivity the coherence resonances were detected through a parametric resonance technique [22]. In addition to the slowly varying DC magnetic field, a small AC component of the magnetic field (oriented along the light propagation axis) was introduced with a secondary coil driven at frequency  $f$ . A lock-in amplifier detected the phase and quadrature components of the photodiode current oscillating at frequency  $f$ . Two different values of  $f$  were used in the measurements. For the cell without buffer gas we used  $f = 75\text{ kHz}$  and for the cell containing Ne  $f = 5\text{ kHz}$  was used. In both cases  $f$  was chosen to exceed the width of the corresponding Hanle resonances. A typical recording of the lock-in output signal as a function of the solenoid DC current is shown in Fig. 3. The central structure of the spectrum corresponds to  $B = 0$ . The spectrum sidebands occurring for  $2\Delta E_Z = hf$  ( $\Delta E_Z$  is the ground state Zeeman energy shift) allow a precise calibration of the magnetic field inside the solenoid.

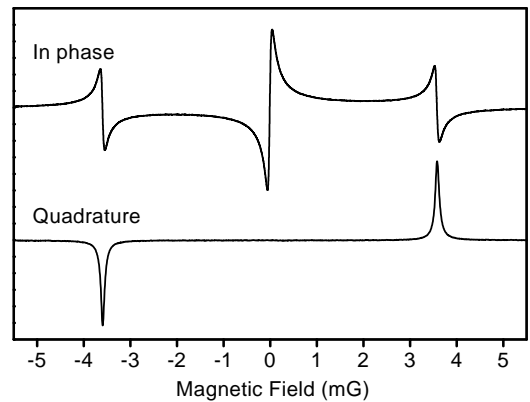


FIG. 3. Experimental parametric resonance signal for the  $F_g = 2 \rightarrow F_e = 1$  transition of  $^{87}\text{Rb}$  in the cell containing buffer gas. Modulation frequency  $f = 5\text{ kHz}$ . The two traces are on the same vertical scale (shifted for clarity).

In the cell containing the buffer gas where the resonances are well resolved (Fig. 3) the parametric resonance scheme used in the experiment allows for isotope selective spectroscopy. For this, the DC magnetic field is kept fixed at the value corresponding to the maximum of one of the (Lorentzian) sidebands resonances observed on the quadrature signal and the quadrature output of the lock-in amplifier is monitored while the frequency of the laser is scanned on the  $D1$  line. Since the resonance condition  $2\Delta E_Z \equiv 2g\mu_B B = hf$  depends on the specific isotope through the gyromagnetic factor  $g$  ( $\mu_B$  is the Bohr magneton), only one isotope contributes to the observed spectrum. An example of such spectrum is shown in Fig. 4 where only the  $D1$  transitions of  $^{87}\text{Rb}$  appear in spite of the cell being filled with natural Rb (72% of  $^{85}\text{Rb}$ ). The gyromagnetic factors of the two hyperfine levels of the ground state of  $^{87}\text{Rb}$  differ in absolute value by less than 0.3%. Consequently all four hyperfine transitions can be observed in the same spectrum. Notice that the hyperfine structure is well resolved in the spectrum of Fig.4. This is a clear indication that in spite of the rather strong collisional regime, the atomic level structure resulting from the hyperfine coupling is preserved and that the total angular momentum  $F_e$  remains a good quantum number. The relative weight of the coherence resonances in the four  $D1$  transitions is appreciated in Fig. 4. The peak corresponding to the  $F_g = 1 \rightarrow F_e = 2$  transition is smaller than that of the  $F_g = 1 \rightarrow F_e = 1$  transition by a factor 25 and is not visible on the scale of Fig. 4. It is worth mentioning that the small  $F_g = 1 \rightarrow F_e = 2$  signal is nevertheless 100 times larger than the residual signal due to the wings of the  $F_g = 1 \rightarrow F_e = 1$  peak estimated from a Gaussian fit.

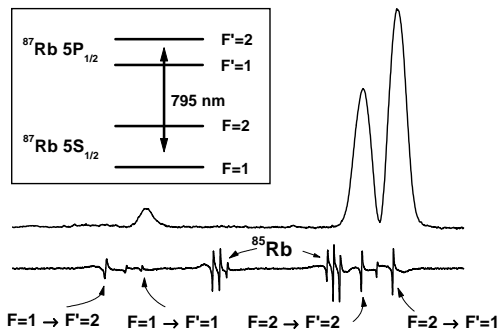


FIG. 4. Quadrature parametric resonance signal as a function of the laser frequency (upper trace). The DC magnetic field is kept fixed at the value corresponding to the positive sideband on Fig. 3. Lower trace: reference saturated absorption signal. Inset: level scheme for the  $D1$  line transitions of  $^{87}\text{Rb}$ .

Figs. 5 and 6 show the observed signals with the laser in resonance with the four  $D1$  transitions in the cell without buffer gas and in the cell containing Ne respectively using the same optical power. The beam diameter was 10 mm and 5 mm respectively. Only the central resonance around  $B = 0$  for the in phase signal is shown in Fig. 6. Without buffer gas the observed resonances have a width which is determined by the time of flight through the optical beam. Notice the sign reversal of the  $F_g = 1 \rightarrow F_e = 2$  transition (EIA) with respect to the three other resonances (EIT). In the cell with buffer gas (Fig. 6), the observed resonances are much narrower as expected from the increase in interaction time due to the diffusive atomic motion. However, under the present experimental conditions the observed linewidth is limited by residual magnetic field inhomogeneities. A sign change is clearly observed for the  $F_g = 1 \rightarrow F_e = 2$  transition with respect to the cell without Ne demonstrating the quenching of the EIA resonance and its reversal into EIT.

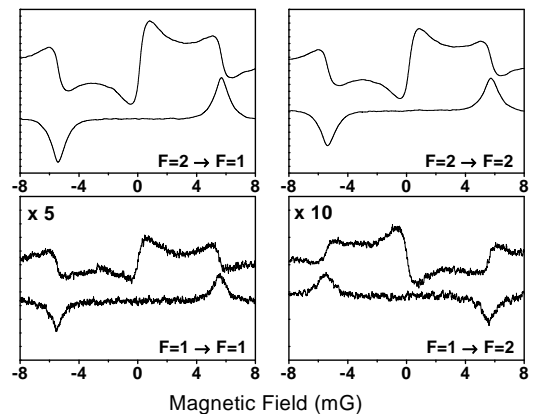


FIG. 5. In phase (upper trace) and quadrature (lower trace) parametric resonance signal for the four hyperfine transitions of the  $D1$  line of  $^{87}\text{Rb}$  in the cell without buffer gas. Comparable vertical scales are used for all curves.

$$+b\Gamma \sum_{q=-1,0,1} Q_{ge}^q \sigma Q_{eg}^q - \gamma\sigma + \gamma\sigma_0 + \gamma_{coll}\bar{\sigma} \quad (1)$$

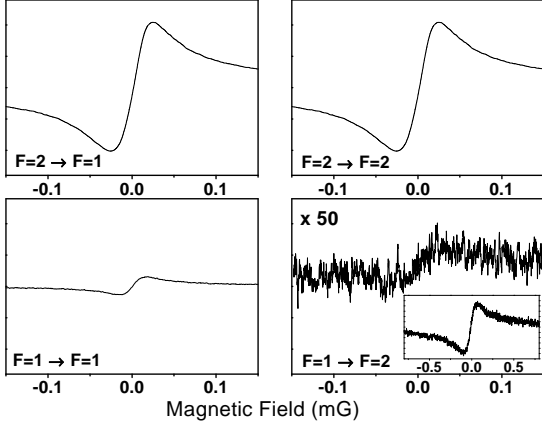


FIG. 6. Central structure of the in phase parametric resonance signal for the four hyperfine transitions of the  $D1$  line of  $^{87}\text{Rb}$  in the cell containing 30 torr of Ne. Comparable vertical scales are used for all curves. The inset shown with the  $F = 1 \rightarrow F = 2$  transition was recorded with increased Rb density.

### III. MODEL

We present in this section a simple theoretical model containing the essential ingredients for the analysis of Hanle/EIT/EIA coherence resonances in DTLS. The model takes explicitly into account the Zeeman degeneracy of the ground and excited states. It considers a unique electric dipole allowed atomic transition in a homogeneous sample of atoms at rest. With respect to the conditions of the experiment, the model contains several simplifications. The effect of the atomic motion, the spatial distribution of the light field, the light propagation in the sample and the influence of neighboring transitions are not considered. Also the effect of collisions is introduced in a quite simplified way through a single collisional relaxation rate as discussed below.

We consider a two-level transition between a ground state  $g$  of angular momentum  $F_g$  and an excited state  $e$  of angular momentum  $F_e$  with energy separation  $\hbar\omega_0$ . The atoms are illuminated by an optical field of amplitude  $E$  and frequency  $\omega$  linearly polarized along the unit vector  $\mathbf{e}$  and submitted to a magnetic field  $B$  perpendicular to  $\mathbf{e}$ . The atoms are submitted to collisions with the buffer gas. It is assumed that the collisions result in dephasing of the atomic optical dipole and can cause real transitions between excited state Zeeman sublevels.

In the frame rotating with the optical field and with the usual rotating wave approximation, the Liouville equation for the density matrix  $\sigma$  of the system is:

$$\dot{\sigma} = -\frac{i}{\hbar} [\hbar\Delta P_e + H_B + V, \sigma] - \frac{(\Gamma + \gamma_{coll})}{2} \{P_e, \sigma\}$$

where  $\Delta = \omega_0 - \omega$ ,  $H_B = -\mu_B F_z (g_g P_g + g_e P_e) B \equiv -M_z B$  is the Zeeman Hamiltonian ( $P_g$  and  $P_e$  are projectors on the ground and excited subspaces respectively,  $g_g$  and  $g_e$  are the gyromagnetic factors of the ground and excited states respectively,  $\mu_B$  is the Bohr magneton and  $\hbar F_z$  the projection of the total angular momentum along the direction of the magnetic field).

The atom field interaction is given by:

$$V = \frac{\hbar\Omega}{2} \mathbf{e} \cdot \mathbf{Q} \quad (2)$$

$\mathbf{Q}$  is a dimensionless vectorial operator related to the electric dipole operator  $\mathbf{D}$  through:

$$\mathbf{D} \equiv \mathbf{Q} \langle F_g \| \mathbf{D} \| F_e \rangle \quad (3)$$

$\Omega \equiv \frac{\langle F_g \| \mathbf{D} \| F_e \rangle E}{\hbar}$  is the reduced Rabi frequency of the optical field ( $\langle F_g \| \mathbf{D} \| F_e \rangle$  is the reduced matrix element of the electric dipole operator for the considered transition).  $Q_{ge}^q = Q_{eg}^{q\dagger}$  are the spherical components of the operator  $P_g \mathbf{Q} P_e$ .  $b$  is a branching ratio coefficient ( $0 \leq b \leq 1$ ).  $\Gamma$  is the spontaneous emission decay rate.  $\gamma$  and  $\gamma_{coll}$  are relaxation rates associated to transit time and excited state collisions respectively.  $\sigma_0 = \frac{P_g}{2F_g+1}$  corresponds to an isotropic density matrix for the ground level with unit total population and  $\bar{\sigma} = \frac{P_e}{2F_e+1} \text{Tr}(P_e \sigma)$  is an (incoherent) isotropic density matrix for the excited state with the same excited state population than  $\sigma$ .

The first term on the r.h.s. of Eq. 1 describes the Hamiltonian evolution of the atom in the presence of the optical and magnetic field. The second term account for the relaxation of the excited state and the optical coherences. In addition to spontaneous emission we consider the relaxation due to collisions with the buffer gas atoms. For simplicity, it is assumed that the effect of buffer gas collisions on optical and Zeeman coherences can be described by the single relaxation rate  $\gamma_{coll}$ . The third term on the r.h.s. of Eq. 1 describes the spontaneous emission transfer of population and coherence from the excited state to the ground state. For open transitions, the branching ratio coefficient  $b$  accounts for the atomic loss due to radiative transitions to external levels ( $b = 1$  corresponds to closed transitions). The fourth term on the r.h.s. of Eq. 1 accounts, in the usual phenomenological way, for the finite interaction time. Although this relaxation term concerns both the ground and the excited level, notice that  $\gamma$  is the only relaxation rate acting on the ground state. The escape of atoms from the interaction region at rate  $\gamma$  is compensated at steady state by the arrival of "fresh" atoms isotropically distributed in the ground state ( $\gamma\sigma_0$  in Eq. 1). The last term on the r.h.s. of Eq. 1 is an effective isotropical repumping term

introduced to compensate the effect of the collisions (included in the second term of the r.h.s. of Eq. 1) on the total excited state population.

The steady state solution of Eq. 1 can be easily obtained numerically [4,5]. The solution of Eq. 1 for conditions corresponding to the parametric resonance scheme where the magnetic field along the light propagation axis is the sum of a DC and a small sine modulated component is presented in the appendix. The calculation of the light absorption signals in phase and in quadrature with respect to the magnetic field modulation are also derived in the appendix.

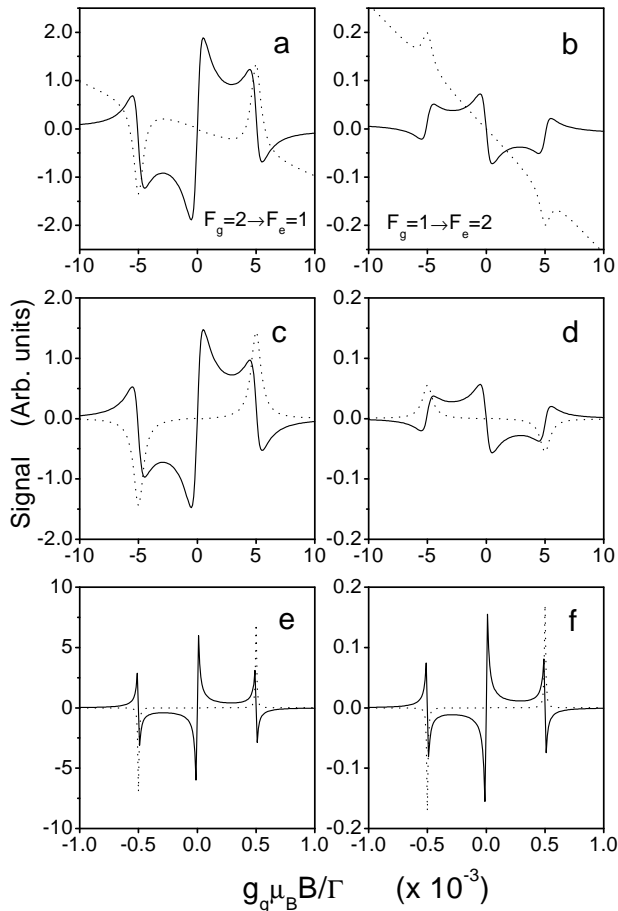


FIG. 7. Calculated signal for the  $F_g = 2 \rightarrow F_e = 1$  (left column) and  $F_g = 1 \rightarrow F_e = 2$  (right column) transitions ( $\Omega = 0.01\Gamma$ ). Solid: in phase signal. Dotted: quadrature signal. *a, b, c, d*:  $\gamma_{coll} = 0$ ,  $\gamma = 10^{-3}\Gamma$ ,  $2\pi f = 10^{-2}\Gamma$ . *e, f*:  $\gamma_{coll} = 4\Gamma$ ,  $\gamma = 10^{-5}\Gamma$ ,  $2\pi f = 10^{-3}\Gamma$ . In *c* and *d* the signal was averaged over  $\Delta$  in the range  $-5\Gamma < \Delta < 5\Gamma$ . The vertical scales are independent for each row but comparable within a row.

The prediction of the model for the transitions of the D1 line of  $^{87}\text{Rb}$  are presented in Fig. 7. Only the  $F_g = 2 \rightarrow F_e = 1$  and  $F_g = 1 \rightarrow F_e = 2$  transitions are

shown. The parameters of the calculation were chosen to correspond approximately to the experimental conditions. The same light intensity is assumed in all figures. We used  $\Omega/\Gamma = 0.01$  (the two transitions shown have the same strength). The branching ratio was taken as  $b = 0.83$  and  $b = 0.5$  respectively (evaluated through standard angular momentum calculus) and the signal corresponding to each transition was weighted proportionally to the thermal occupation number of the lower level (coefficients  $5/8$  and  $3/8$  respectively). The plots a-d in Fig. 7 correspond to the absence of collisions. In these plots the transit time relaxation rate was taken as  $\gamma = 10^{-3}\Gamma$ . While plots a,b,e,f correspond to the direct output of our model for  $\Delta = 0$ , plots c and d correspond to the signal averaged over  $\Delta$  in the range  $-5\Gamma < \Delta < 5\Gamma$  to include the contribution of different velocity classes to the signal ( $\Delta = -kv$ ,  $k$  is the wavevector and  $v$  the velocity). When different from zero, the collisional rate was taken as  $\gamma_{coll} = 4\Gamma$  a value estimated from the data in [19]. The precise value of  $\gamma_{coll}$  has small influence on the lineshape of the signal provided that it is taken sufficiently larger than  $\Gamma$ . Notice the sign reversal on the calculated signal corresponding to the  $F_g = 1 \rightarrow F_e = 2$  transition when  $\gamma_{coll} \neq 0$  with respect to the case in which  $\gamma_{coll} = 0$ .

#### IV. DISCUSSION.

In spite of the simplicity of the model, the main features of the experimental observations are well reproduced in the calculated spectra (similar agreement is obtained for the two hyperfine transitions not shown). The variation in the amplitude of the signal between the two hyperfine transitions is essentially the consequence of the different values of the branching ratio  $b$ . In the plots a and b of Fig. 7 a non resonant contribution is clearly visible giving rise to the observed slope in the quadrature signal. Such non resonant contribution is negligible on the scale of plots e and f. We attribute this difference to the fact that the non resonant contribution originates in the linear response of the atomic sample while the resonances are due to its nonlinear response. In an open two level system, the saturation intensity  $\Omega_S^2$  is of the order of  $\gamma\Gamma$ . With the values of  $\gamma$  used in the two cases considered above, we have  $\Omega < \Omega_S$  for the pure Rb vapor (plots a - d) and  $\Omega > \Omega_S$  for plots e and f. This explains the different relative weight of the linear and nonlinear contributions in the two cases. Since the coherence resonance condition is essentially Doppler-free, only when  $\Omega < \Omega_S$  the integration over different detunings  $\Delta$  (integration over velocity classes) result in a significant change in the lineshape. After integration, the nonresonant background is cancelled (assuming that the laser is centered on the Doppler profile) in agreement with the experimental observation.

Several simplifications were assumed in the theoretical model. The approximation consisting in considering an homogeneous sample of atoms at rest have already been addressed; when necessary this simplification can be abandoned carrying on the integration over velocity classes as described above. Another important approximation is the simplified treatment of the collisional process described through a unique scalar rate. Also, it is assumed in the model that the atom remain confined to the excited state level during the collisional process. However, for the Ne density used in the experiment, inelastic collisions have a non-negligible probability and a fraction of the excited atoms may be collisionally transferred to a different excited hyperfine level or even to the  $5P_{3/2}$  manifold [19]. In any case, such inelastic processes are not expected to preserve the Zeeman coherence of the excited levels. The overall consequence of the inelastic collision processes, followed by spontaneous emission, is to provide a second (indirect) path for the return of the atoms to the ground state. With the assumption that this additional decay channel is isotropic its contribution can be effectively included in the collisional rate  $\gamma_{coll}$ .

## V. CONCLUSIONS.

We have studied Hanle/EIT and Hanle/EIA resonances on the  $D1$  line of  $^{87}\text{Rb}$  vapor both in absence and in presence of a buffer gas. The coherence resonances were studied through a parametric resonance technique. We observed that the Hanle/EIA resonance, occurring for the  $F_g = 1 \rightarrow F_e = 2$  transition, change sign in the presence of a buffer gas as a consequence of collisions in the excited state. A theoretical model was presented that allows the numerical calculation of the parametric resonance signals. In spite of its simplicity, the model reproduces the essential features of the experimental results on the assumption that the collision of the Rb atoms with the buffer gas result in the isotropic decoherence of the excited state. The overall agreement between the experimental results and the simple model clearly suggest that the preservation of the excited state coherence during the excited state lifetime and its transfer to the ground state are, as suggested in [6], key ingredients for the occurrence of EIA.

## VI. ACKNOWLEDGMENTS.

The authors are thankful to D. Bloch for fruitful discussions. This work was supported by the Uruguayan agencies: CONICYT, CSIC and PEDECIBA and by ECOS (France).

## VII. APPENDIX.

In this appendix we describe the calculation of the parametric resonance signals.

We consider the evolution of the atom-optical field system under the influence of a longitudinal magnetic field of the form:

$$B = B_0 + B_1 \cos(\delta t) \quad (4)$$

We seek a solution for the density matrix on the form:  $\sigma(t) \simeq \sigma^0 + \sigma^1(t)$  where  $\sigma^0$  is constant and  $\sigma^1(t)$  is a time dependent correction to first order in  $B_1$ . Substituting in Eq. 1, we have:

$$0 = -\frac{i}{\hbar} [\hbar\Delta P_e - M_z B_0 + V, \sigma^0] - \frac{(\Gamma + \gamma_{coll})}{2} \{P_e, \sigma^0\} + b\Gamma \sum_{q=-1,0,1} Q_{ge}^q \sigma^0 Q_{eg}^q - \gamma\sigma^0 + \gamma\sigma_0 + \gamma_{coll}\overline{\sigma^0} \quad (5)$$

$$\dot{\sigma}^1 = -\frac{i}{\hbar} [\hbar\Delta P_e - M_z B_0 + V, \sigma^1] + \frac{i}{\hbar} [M_z B_1, \sigma^0] \cos(\delta t) - \frac{(\Gamma + \gamma_{coll})}{2} \{P_e, \sigma^1\} + \gamma_{coll}\overline{\sigma^1} + b\Gamma \sum_{q=-1,0,1} Q_{ge}^q \sigma^1 Q_{eg}^q - \gamma\sigma^1 \quad (6)$$

If one identifies the matrix elements of  $\sigma^0$  and  $\sigma^1$  with the components of column vectors  $Y^0$  and  $Y^1$ , then Eqs. 5 and 6 can be rewritten as:

$$\mathcal{M}Y^0 = P \quad (7)$$

$$\dot{Y}^1 = \mathcal{M}Y^1 + A \cos(\delta t) \quad (8)$$

where  $\mathcal{M}$  is a matrix with time independent coefficients and  $P$  and  $A$  are two column vectors associated to  $\gamma\sigma_0$  and  $\frac{i}{\hbar} [M_z B_1, \sigma^0]$  respectively.

We are interested in the solution of Eq. 8 of the form:

$$Y^1(t) = \alpha \cos(\delta t) + \beta \sin(\delta t) \quad (9)$$

after substitution in Eq. 8 one gets:

$$\alpha = \mathcal{M}(\delta^2\mathbb{I} + \mathcal{M}^2)^{-1} A \quad (10)$$

$$\beta = \delta(\delta^2\mathbb{I} + \mathcal{M}^2)^{-1} A$$

where  $\mathbb{I}$  is the identity matrix.

After numerical evaluation of vectors  $\alpha$  and  $\beta$  one can retrieve the corresponding density matrices  $\sigma_\alpha$  and  $\sigma_\beta$  and the corresponding light absorption coefficients respectively in phase and in quadrature with the magnetic field modulation:

$$\lambda_i \propto \text{Im}[\mathbf{e} \cdot \text{Tr}(\sigma_i \mathbf{D})] \quad (i = \alpha, \beta) \quad (11)$$

- [1] For a general overview of coherent processes see M.O. Scully and M.S. Zubairy, *Quantum Optics*, Cambridge University Press, Cambridge (1997) and references therein.
- [2] see S. E. Harris, *Physics Today*, **50**(7) 36 (1997) and references therein.
- [3] A.M. Akulshin, S. Barreiro and A. Lezama, *Phys. Rev. A* **57**, 2996 (1998).
- [4] A. Lezama, S. Barreiro and A.M. Akulshin, *Phys. Rev. A* **59**, 4732 (1999).
- [5] A. Lezama, S. Barreiro, A. Lipsich and A.M. Akulshin, *Phys. Rev. A* **61**, 013801 (2000).
- [6] A.V. Taichenachev, A.M. Tumaikin and V.I. Yudin, *Phys. Rev. A* **61**, 011802 (2000).
- [7] P. Valente, H. Failache and A. Lezama, arXiv:quant-ph/0209011.
- [8] F. Renzoni, W. Maichen, L. Windholz and E. Arimondo, *Phys. Rev. A* **55**, 3710 (1997).
- [9] F. Renzoni and E. Arimondo, *Phys. Rev. A* **58**, 4717 (1998).
- [10] F. Renzoni, A. Lindner and E. Arimondo, *Phys. Rev. A* **60**, 450 (1999).
- [11] Y. Dancheva, G. Alzetta, S. Cartaleva, M. Taslakov and Ch. Andreeva, *Opt. Commun.* **178**, 103 (2000).
- [12] F. Renzoni, S. Cartaleva, G. Alzetta and E. Arimondo, *Phys. Rev. A* **63**, 065401 (2001).
- [13] G. Alzetta, S. Cartaleva, Y. Dancheva, Ch. Andreeva, S. Gozzini, L. Botti and A. Rossi, *J. Opt. B: Quantum Semiclass. Opt.* **3**, 181 (2001).
- [14] W. Happer, *Rev. Mod. Phys.* **44**, 169 (1972) and references therein.
- [15] S.Brandt, A. Nagel, R. Wynands and D. Meschede, *Phys. Rev. A* **56**, 1063 (1997).
- [16] M. Erhard, S. Nußmann and H. Helm, *Phys. Rev. A* **62**, 061802 (2000).
- [17] M. Erhard and H. Helm, *Phys. Rev. A* **63**, 043813 (2001).
- [18] A. Gallagher, *Physical Review* **157**, 68 (1967).
- [19] B.R. Bulos and W. Happer, *Phys. Rev. A* **4**, 849 (1971).
- [20] W. Kedzierski, J. Gao, W.E. Baylis and L. Krause, *Phys. Rev. A* **49**, 4540 (1994).
- [21] M.D. Rotondaro and G.P. Perram, *Phys. Rev. A* **58**, 2023 (1998).
- [22] J. Dupont-Roc, *Rev. Phys. Appl.* **5**, 853 (1970).